Engineering and Technology Journal e-ISSN: 2456-3358

Volume 09 Issue 04 April-2024, Page No.- 3763-3771

DOI: 10.47191/etj/v9i04.14, I.F. – 8.227

Satellite Image Analysis Approach for Identifying Flood Impacts in DKI Jakarta

Mohamad Mahfudz[1], Bambang Riadi[2], Rian Nurtyaman[3], Prasetyo Putro Utomo[4]

[1,2,3,4] Geodetic Engineering, Pakuan University, Bogor, 16143, Indonesia

ABSTRACT: Jakarta, as the capital city of Indonesia, is one of the major cities in the world that is inevitably affected by disasters resulting from climate change. The topographical characteristics of Jakarta, situated in a low-lying area, make it susceptible to floods during the rainy season. In 2020, Jakarta experienced a rainfall of 377 mm/day, marking the highest precipitation during the period of 1866 to 2020. To mitigate the impact of flood disasters, the availability of flood distribution data is crucial. The process of identifying flood distribution utilizes Sentinel-1 radar satellite imagery with the Normalized Difference Sigma-Naught Index (NDSI) method. NDSI is sensitive to open water bodies due to changes in land surface properties during floods. Based on NDSI analysis, the flood distribution in DKI Jakarta was identified on January 2, 2020, covering 17,38% of the total area of DKI Jakarta, which is 661,52 km2.

KEYWORDS: Flood Distribution, Sentinel-1, DKI Jakarta, NDSI

I. INTRODUCTION

Floods are the most frequently occurring disasters in Indonesia, causing losses to communities and environmental damage. Floods are triggered by various factors, including hydrometeorological, topographical, geological, soil, and human activities (Nucifera and Putro, 2018; Mahfudz et al., 2022). One of the hydrometeorological disasters is rainfall-induced flooding, with excessive rainfall occurring across most of Indonesia during the year 2010, even during the dry season from June to August (Yulihastin, 2011). Floods manifest in two ways: 1) river overflow caused by river discharge exceeding the river's capacity during heavy rainfall, and 2) inundation in low-lying flat areas that are typically not submerged (Ariyora et al., 2015).

Jakarta is situated on the northern coast of Java, forming a delta with 13 rivers connected to Jakarta Bay. Topographically, Jakarta is located in a low-lying area, with nearly 40% of its area below sea level. Floods in Jakarta can be categorized into local floods, upstream floods, and tidal floods. Local floods result from intense rainfall within the city, exceeding the capacity of existing drainage systems. Upstream floods occur due to significant runoff from rivers originating in the Bogor Regency. Tidal floods are caused by high tides and rising sea levels due to global climate change (Kardhana, 2013). The causes of flooding in Jakarta are not only due to rainfall but also result from land subsidence, rising sea levels, and natural disasters (Wijayanti et al., 2017) The classification of Jakarta's landforms based on their origin includes fluvial, fluvial-coastal, and coastal landforms. The landforms are characterized by layers of volcanic-fluvial sedimentary rock, especially along the rivers. The topography ranges from gentle to flat with low elevations, even in coastal alluvial plain areas below sea level. Besides these landforms, other landforms exist in the northern part of Jakarta, such as coastal ridges parallel to the coastline (Tambunan, 2017).

According to BPDB DKI Jakarta in 2022, the intensity and precipitation evenly spread across all DKI Jakarta areas during the period of January 18 (at 07:00 WIB) to January 19 (at 07:00 WIB) were categorized as extreme, exceeding 150 mm per day. The Meteorology, Climatology, and Geophysics Agency (BMKG) recorded a daily rainfall intensity of 204 mm at the Kemayoran Meteorological Station. This marked the highest rainfall in Jakarta during the period from November 2021 to January 18, 2022. Among the 13 rivers crossing Jakarta, the Ciliwung River contributes the most to the potential occurrence of floods in the DKI Jakarta region. According to NEDECO (1973), the Ciliwung River Basin covers approximately 347 km2, the largest among the river basins (Harsoyo, 2013). The planned 50-year return period discharge for the Ciliwung River Basin is 261.397 m3/s, while the planned 100-year return period discharge is 307.012 m3/s (Wigati and Soedarsono, 2016). The Ciliwung River Basin faces issues such as the high rate of land cover change from Green Open Space (Ruang Terbuka Hijau, RTH) to built-up areas. In 1990, the largest land cover change in the area was in built-up areas (52.76%), Green Open Space (RTH) (33.75%), and water bodies (13.49%). By 2000, the RTH area decreased to 27.07%, while the built-up area increased to 61.05%. The most significant change to built-up areas occurred in the downstream area, reaching 80.00%

(Aslinda and Syartinilia, 2017). The Jakarta Canal Flood is a water collection channel that is an integral part of the Ciliwung River. The collector channel will accommodate overflow from the Krukut and Cideng Rivers, which then flows into the sea. This water system is the lifeline for controlling floods in Jakarta (Taufik et al., 2022).

II. METHOD

Research Location

Jakarta, with an area of 661.52 km2, is located between 6°8' South Latitude and 106°48' East Longitude. It borders Banten Province to the west and West Java Province to the east, south, and north, with the northern boundary facing the Java Sea. Administratively, DKI Jakarta Province is divided into 5 municipalities and 1 Administrative District, namely Jakarta Pusat with a land area of 47.90 km2; Jakarta Utara with a land area of 154.01 km2, Jakarta Barat with a land area of 126.15 km2; Jakarta Selatan with a land area of 145.73 km2; Jakarta Timur with a land area of 187.73 km2, and the Administrative District of thousand islands.

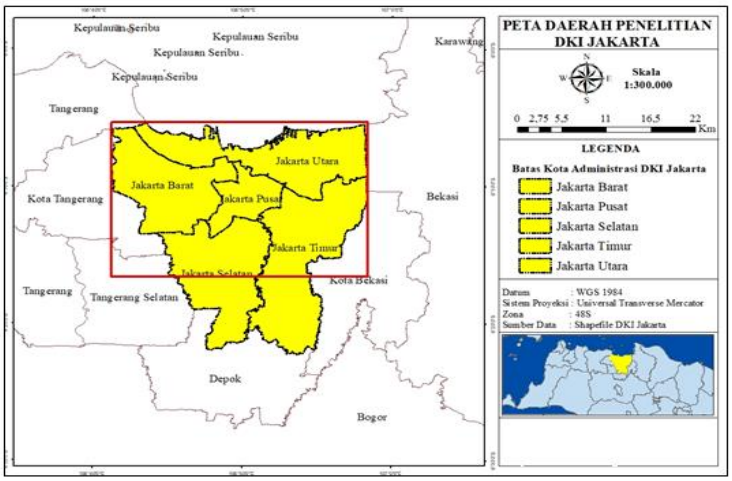

Figure 1 : Research Location

Spatial analysis is highly effective in the processing and analysis of data, expediting the decision-making process in the studied field. In this research, data collection is the initial step, followed by the data analysis process to obtain results and validation processes. To clarify the research flow, it is presented in the flowchart in Figure 2.

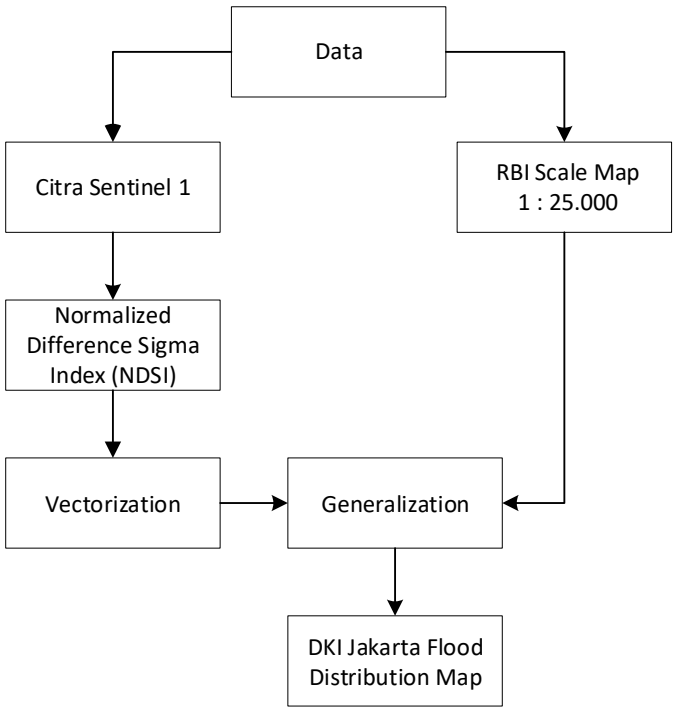

Figure 2 : Research Flow Diagram

Synthetic Aperture Radar (SAR) operates at wavelengths unaffected by cloud cover or lack of illumination, allowing it

to acquire data through a location both day and night, and under all weather conditions. The C-SAR instrument of Sentinel-1 provides reliable and repetitive monitoring of large areas. Sentinel-1 includes C-band imaging operating in four exclusive imaging modes with different resolutions (up to 5 m) and ranges (up to 400 km) (Filipponi, 2019). The data used in this study are radar satellite images from Sentinel-1 recorded on August 11, 2019, and January 2, 2020, with VV (vertical-vertical) polarization, along with other spatial supporting data such as the administrative boundaries of the Jakarta Capital Region in .shapefile format (GIS BPBD DKI Jakarta), as indicated in Table 1.

Table 1: Citra Sentinel 1 Characteristics

Characteristics	Citra 11-08-2019	Citra 02-01-2020
Setellite name	Sentinel-1	Sentinel-1
Satellite number	A	A
Scene	S1A_IW_GRDH_1SDV_20190811T111515_20190811T111540_028520_03397F_CEB8.SAFE	S1A_IW_GRDH_1SDV_20200102T111515_20200102T111540_030620_038227_CF59.SAFE
Instrument	SAR-C	SAR-C
Acquisition date	11-AUG-2019 11:15:15:756Z	02-JAN-2020 11:15:15.986Z
Mode	IW	IW
Pass direction	Ascending	Ascending
Antenna pointing	Right	Right
Polarisation	VV, VH	VV, VH
Product level	L1	L1
Product type	GRD	GRD

Apply Orbit File

The orbital vector information in SAR product metadata is generally inaccurate. The accurate satellite orbit is determined after a few days and becomes available from a few days to a week after the product is produced. The precise orbit file application available in SNAP allows for automatic downloading and updating of orbit vector status for each SAR location in its metadata, providing accurate satellite position and velocity information (Mangidi et al., 2023)

Thermal Noise Removal

Sentinel-1 image intensity typically experiences interference in cross-polarization channels (Park et al., 2018). Thermal Noise Removal is one step to reduce noise effects on SAR image texture by normalizing backscatter signals in Sentinel-1 images. Sentinel-1 Level-1 products provide a Look-Up Table (LUT) for each measurement data set to obtain a calibrated noise profile according to GRD-calibrated data.

Calibrate

SAR image calibration aims to assign pixel values to the image after backscatter in accordance with conditions on the Earth's surface. The calibration process for Sentinel-1 images involves radiometric correction, which is a fundamental correction to eliminate noise resulting from image distortion due to sunlight position (Rahayu & Candra, 2014). Radiometric correction aims to adjust pixel values to their expected values, considering atmospheric interference as a primary error source. Atmospheric effects cause the reflected values of objects on the Earth's surface recorded by the sensor to deviate from their true values, either becoming larger due to scattering or smaller due to absorption processes (Lukiawan et al., 2019).

Speckle Filtering

Satellite images sometimes contain noise that obscures part of the surface information, affecting the interpretation process. One such noise in SAR images is speckle, appearing as white spots, often referred to as "salt and pepper," which can decrease interpretability by covering surface information in the image (Dasari et al., 2016). Speckle Filtering is a process to improve image quality by removing speckle. The Lee speckle filter method is used in this research, based on Minimum Mean Square Error (MMSE) and geometric aspects. Lee's statistical filter is one of the most popular and well-known speckle removal techniques in radar image processing (Rubel et al., 2021).

Terrain Correction

Terrain Correction is used to correct the geometry of images distorted by surface positions (Assidiq and Rokhmana, 2021). Geometric information involves spatial distribution-related geographic positions. Geometric data includes geo-referenced data, both in terms of position (latitude and longitude coordinate system) and information contained within. According to Mather (1987), geometric correction transforms remote sensing images so that they have map-like properties in terms of form, scale, and projection (Lukiawan et al., 2019). The Terrain Correction or geometric correction method used in this study is the Range Doppler Terrain

Correction method, which implements orthorectification to geocode SAR from radar geometry to obtain projectable results.

Normalized Difference Sigma Index (NDSI)

In 2011, Furuta and Tomiyama developed the Normalized Difference Sigma-Naught Index (NDSI) for surface change detection (e.g., landslides) using SAR images. This index is obtained by calculating the normalized difference in sigma-naught values between two SAR images. NDSI can be calculated using the formula :

$$NDSI = \frac{\sigma^{m}_{o} - \sigma^{s}_{o}}{\sigma^{m}_{o} - \sigma^{s}_{o}} \quad (1)$$

Where :

σ^0 = is the sigma naught

m = is the master, and

s = is the slaves.

NDSI values range from -1 to 1, where values approaching 1 or -1 indicate significant changes in surface properties or the imaged object. On the other hand, when NDSI values approach zero, it can be concluded that the target has not undergone significant changes. Additionally, NDSI is sensitive to open water bodies because changes in land surface properties during flooding transform it into a specular surface that reflects SAR signals away from the satellite, dramatically reducing backscattering coefficients, resulting in NDSI values approaching -1. Another advantage of using NDSI is derived from the fact that it is a normalized difference that can be described with a Gaussian distribution and has a common scale, allowing for multi-temporal data comparison (Ulloa et al., 2020).

III. RESULTS AND DISCUSSION

The data processing process for mapping the distribution of floods in Jakarta, based on Sentinel-1 images comparing two different conditions, during a flood and non-flood, was conducted. This comparison was based on media reports of the flood event on January 2, 2020, and non-flood Sentinel-1 images on August 11, 2019. The images were downloaded from the website www.scihub.copernicus.eu, as shown in Figure 3 :

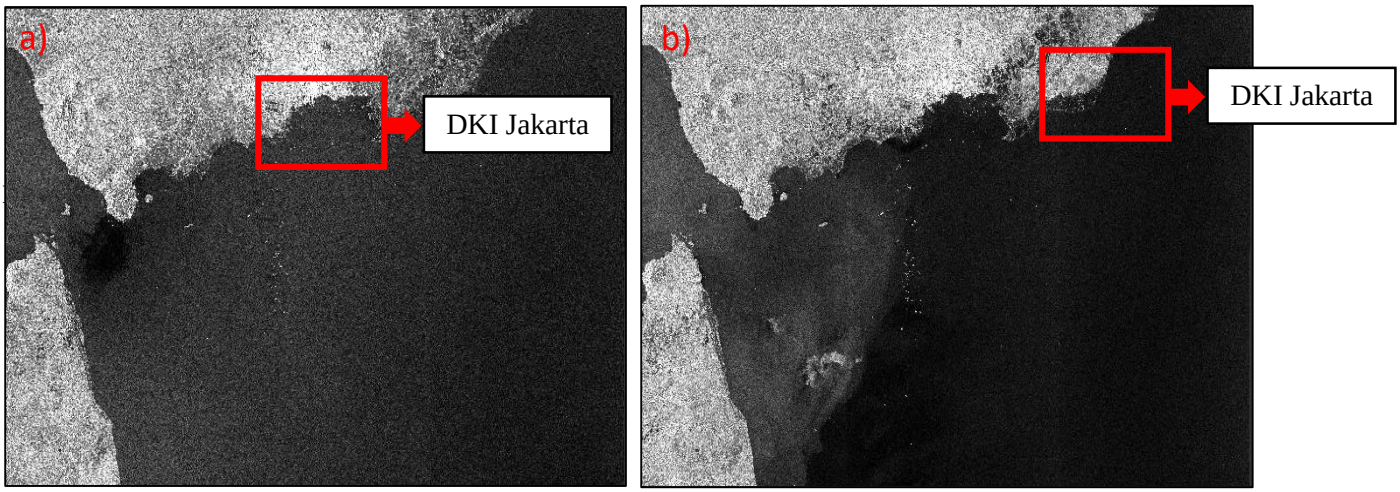

Figure 3 : a) sentinel image on August 11, 2019 b) Sentnel-1 Image on January 2, 2020

Identification of flood distribution using the NDSI method allows us to observe differences in phenomena at different times. The expression in the band maths expression is obtained through the following calculations :

Band Maths Expression :

$$\frac{(Sigma0\_VV\_mst\_11Aug2019 - Sigma0\_VV\_slv1\_02Jan2020)}{(Sigma0\_VV\_mst\_11Aug2019 + Sigma0\_VV\_slv1\_02Jan2020)}$$

The results of the band math expression calculation on Sentinel-1 images are visualized as shown in figure 4 below :

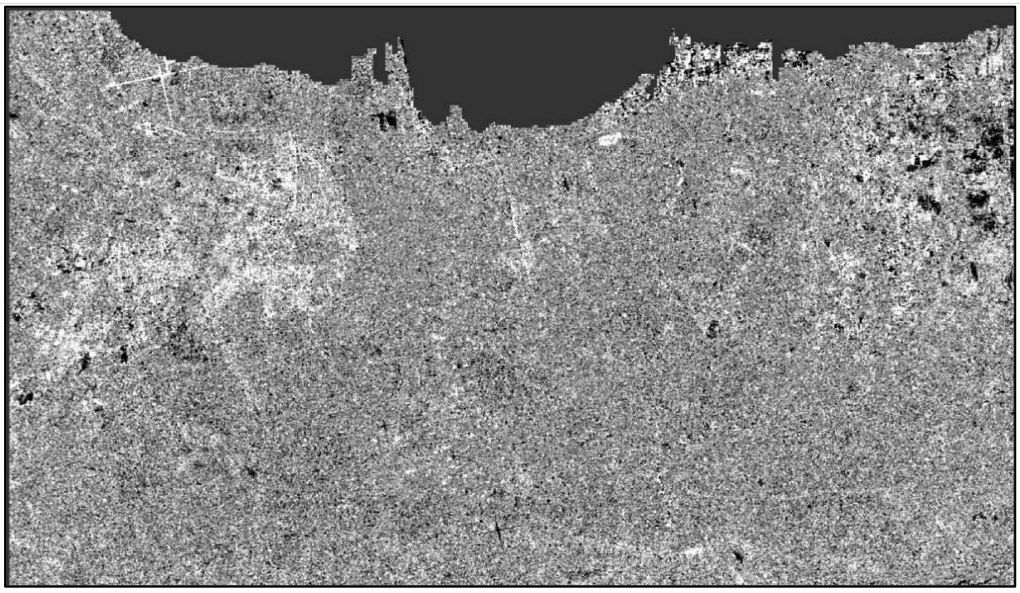

Figure 4 : NDSI Calculation Results

The process of identifying flood distribution involves identifying pixels using pixel information. Pixel information refers to data or information related to individual pixels in a digital image. A pixel is the basic element of a digital image, and each pixel represents a specific color or intensity. Pixel information includes various attributes such as color values, brightness levels, or other information that can be used to analyze and process images. In the context of flood distribution identification, pixel information can include visual characteristics related to water or submerged areas. For example, changes in color, low brightness levels, or specific patterns in pixels can indicate that an area is affected by a flood.

The process of identifying flood distribution using pixel information involves analyzing pixel attributes to determine the location and extent of the flood-affected area. In this research, the expression **(ChangeIndex > 0.5) * 255** is used. The value 0.5 is obtained by identifying pixel values that appear white in the image after the NDSI process. This result only provides information about the distribution of the flood in raster data format. In Figure 5, the visualization of the flood distribution is shown, identified by the color white.

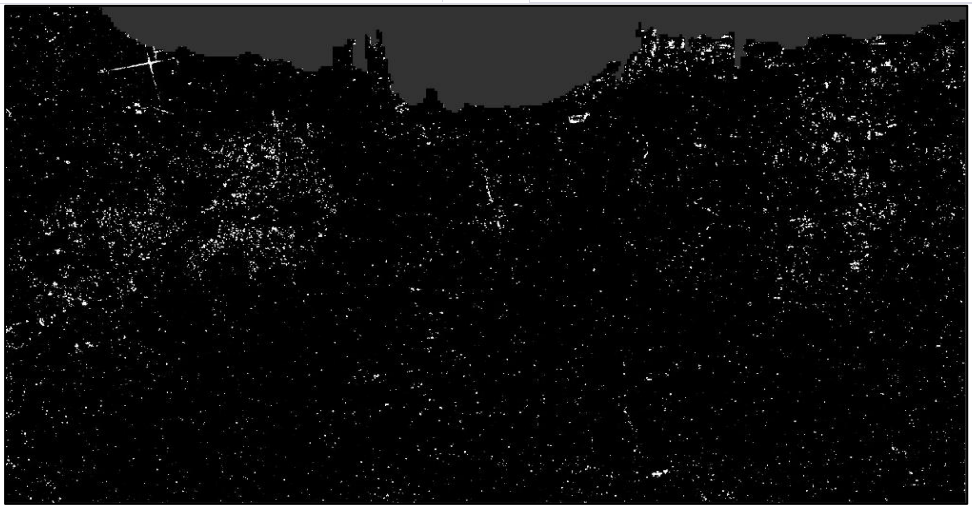

Figure 5 : Flood Distribution on January 2, 2020, in Some Parts of DKI Jakarta

Vectorization and Generalization

Vectorization of an image is the process of converting a raster image, consisting of pixels, into a vector representation consisting of geometric objects such as lines, curves, and polygons. The conversion from raster to vector involves overlaying the rasterized shapes, where the grid cell size for the now vectorized file is the same as the raster file. Using these cells, Russell calculates the area of each newly converted polygon by adding the number of cells occupied by each polygon and multiplying the result by the grid cell size. It is important to note that area measurement is crucial as it helps determine how much data is lost, thus determining the accuracy of raster to vector in GIS after rasterizing vector shapes https://www.rastertovector.com/articles/gis-raster-to-vector-accuracy/.

Map generalization is a process of simplification caused by the reduction or derivation of a map from a large scale to a smaller one while retaining the main characteristics of the map. Generalization is necessary because not all elements on a map at a particular scale can be fully displayed at a smaller scale (due to the increasing density of map content, limited minimum visibility capability of the eye at 0.02 mm at a distance of 30 cm from the eye, minimum size of important objects that must be displayed, and clear differences in shape) (Hisanah et al., 2015). Vector map generalization is the process of simplifying and removing certain details in a vector map with the aim of improving clarity, readability, or reducing complexity. The main goal of map generalization is to produce an effective and informative map without losing meaning or important information.

The conversion from raster to vector is done to obtain information about the flood area. In this process, the area classification is performed for areas of 1 hectare or more, followed by generalization. After the vectorization process, generalization is carried out using values such as Aggregation Distance of 100 Meters, Minimum Area of 2 Hectares, and Minimum Hole Size of 2 Hectares. Figure 6 shows the visualization of the flood distribution in the DKI Jakarta area on January 2, 2020, based on administrative boundaries.

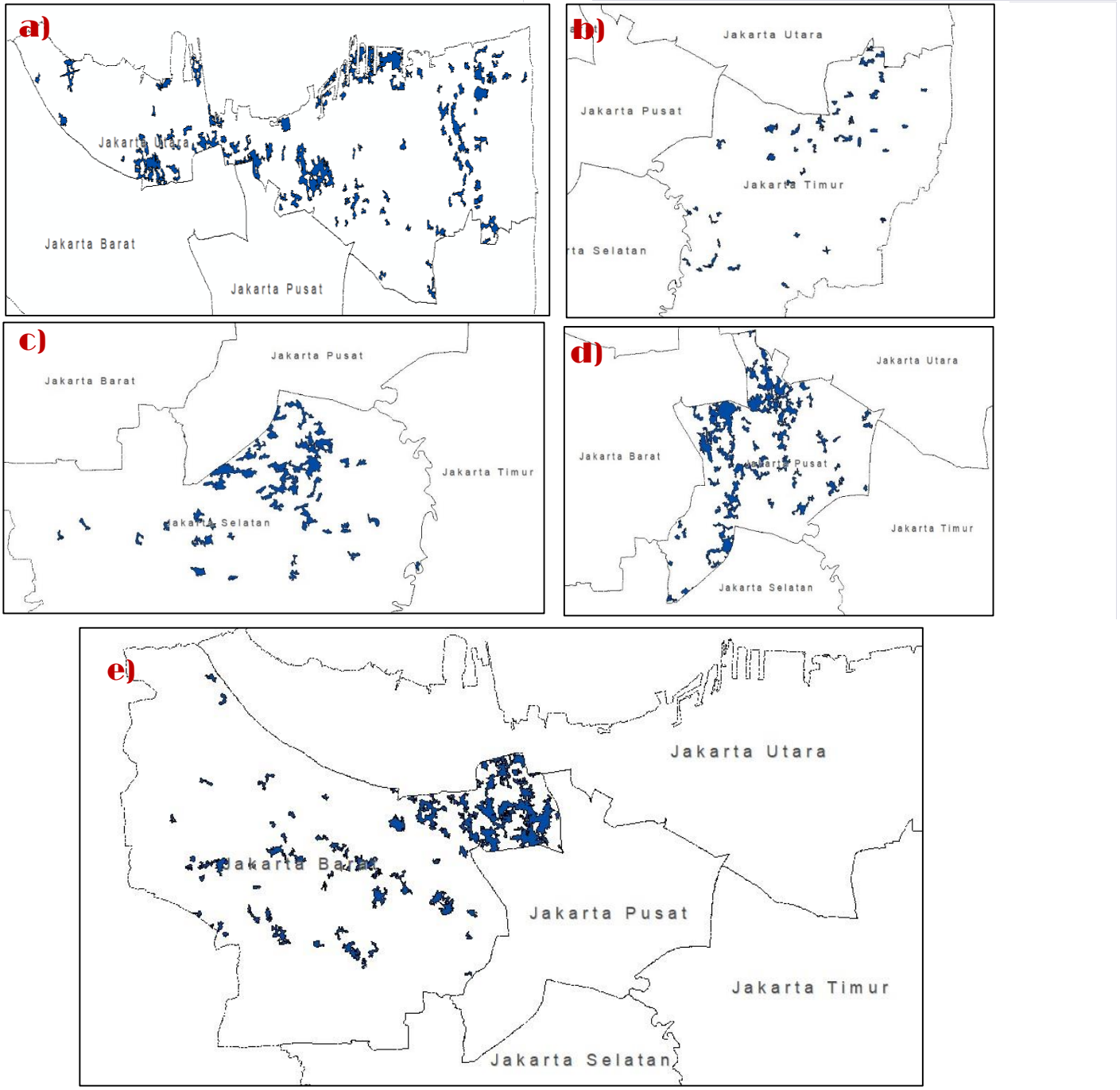

Figure 6 : a) Flood Distribution in North Jakarta b) Flood Distribution in East Jakarta
c) Flood Distribution in Shout Jakarta d) Flood Distribution in Center Jakarta
e) Flood Distribution in West Jakarta

The percentage of each region based on administrative boundaries for North Jakarta had the widest flood distribution compared to other regions, namely 7 .61%, East Jakarta flood distribution area has an area of at least 0.99%. For the other areas, West Jakarta's flood distribution reached 5.6%, while Central Jakarta's area was 1.22% and South Jakarta's area was 1.98%. Meanwhile, the area of each region is based on the administrative boundaries of DKI Jakarta as shown in table 2, while the visualization map of the overall flood distribution area is shown in figure 7:

Table 2 : Flood Distribution Area in DKI Jakarta on January 2, 2020

Administrative Area	Flood Area (km)
North Jakarta	11,1687
East Jakarta	1,8176
South Jakarta	3,0614
Central Jakarta	6,3648
West Jakarta	7,2199

Source : Data Analysis

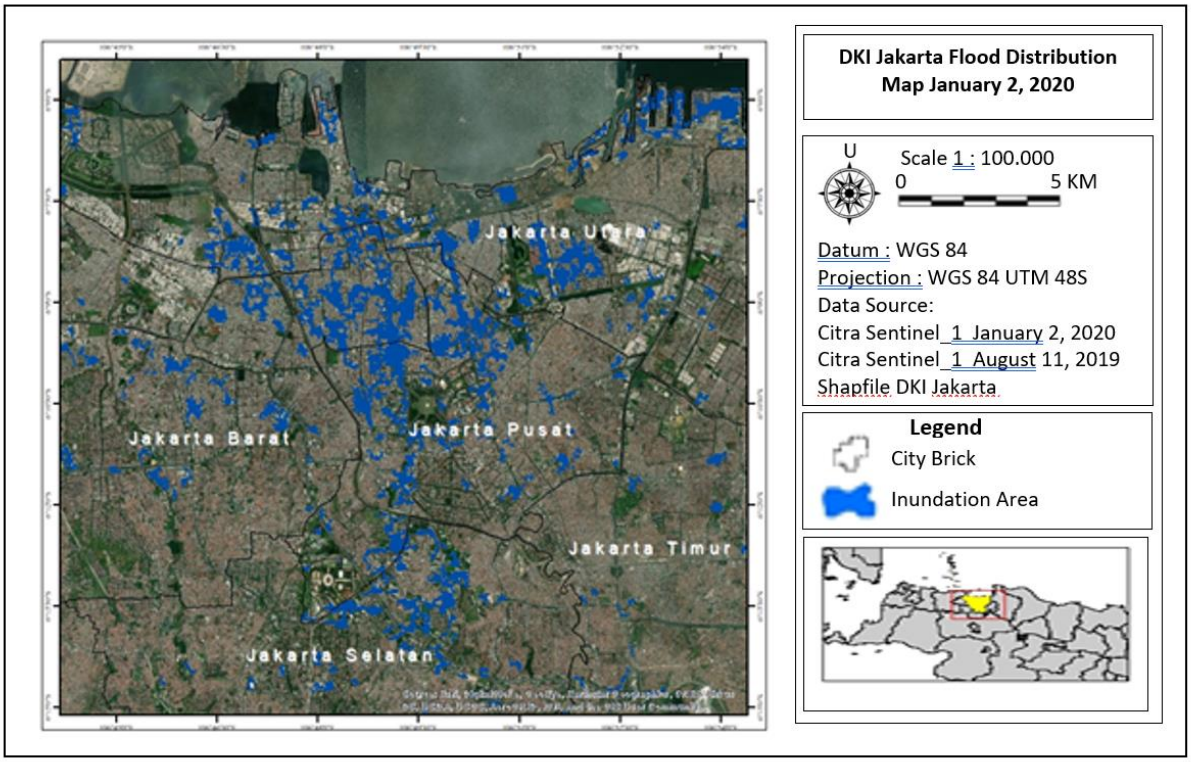

Figure 7 : Flood Distribution on January 2, 2020, in Some Parts of DKI Jakarta

IV. CONCLUSION

The utilization of Sentinel-1 imagery in this study has provided high accuracy in mapping the distribution of floods in DKI Jakarta. The imagery is capable of offering detailed information about water surface conditions and can be effectively used for flood monitoring. Sentinel-1 imagery also demonstrates timely precision in flood monitoring. With its high temporal resolution, it can provide real-time or near real-time information, making it an effective tool for decision-making in flood disaster management. The percentage of flood-affected area, amounting to 17,38 % of the total area of DKI Jakarta, indicates a significant impact of the flood event on January 2, 2020. This underscores the need for serious attention to flood disaster mitigation in the metropolitan region.

V. ACKNOWLEDGMENTS

We extend our gratitude to the Research and Community Service Institute (LPPM) of Unpak for supporting this research activity. We would also like to express our thanks to Copernicus, the National Institute of Aeronautics and Space (BIG), and the Jakarta Provincial Government for providing online data, enabling the successful implementation of this research project.

REFERENCES

1. Ariyora, Y. K. S., Budisusanto, Y., & Prasasti, I. (2015). Pemanfaatan Data Penginderaan Jauh Dan Sig Untuk Analisa Banjir (Studi Kasus : Banjir Provinsi Dki Jakarta). *Geoid*, *10*(2), 137. https://doi.org/10.12962/j24423998.v10i2.805
2. Aslinda, N., & Syartinilia, . (2017). Kajian Perubahan Lahan Menjadi Permukiman Dan Karakteristiknya Di Daerah Aliran Sungai (Das) Ciliwung Bagian Hilir. *Jurnal Lanskap Indonesia*, *8*(1), 38–49. https://doi.org/10.29244/jli.v8i1.16610
3. Assidiq, H. F., & Rokhmana, C. A. (2021). Hubungan Dual Polametric SAR Band – C dan Landsat 8 untuk Identifikasi Potensi Kekeringan. *Geoid*, *16*(2), 248. https://doi.org/10.12962/j24423998.v16i2.8581
4. Braun, A., & Veci, L. (2021). SENTINEL-1 Toolbox SAR Basics Tutorial. *Esa*, *March*, 1–20.
5. Dasari, K., Anjaneyulu, L., Jayasri, P. V., & Prasad, A. V. V. (2016). Importance of speckle filtering in image classification of SAR data. *2015 International Conference on Microwave, Optical and Communication Engineering, ICMOCE 2015*, *December*, 349–352. https://doi.org/10.1109/ICMOCE.2015.7489764
6. Filipponi, F. (2019). *Sentinel-1 GRD Preprocessing Workflow*. 11. https://doi.org/10.3390/ecrs-3-06201
7. Furuta, R., & Tomiyama, N. (2011). A study of detection of landslide disasters due to the pakistan earthquake using ALOS data. *34th International Symposium on Remote Sensing of Environment - The GEOSS Era: Towards Operational Environmental Monitoring*, *1*.
8. Harsoyo, B. (2013). Mengulas Penyebab Banjir Di Wilayah DKI Jakarta Dari Sudut Pandang Geologi, Geomorfologi Dan Morfometri Sungai. *Jurnal Sains & Teknologi Modifikasi Cuaca*, *14*(1), 37. https://doi.org/10.29122/jstmc.v14i1.2680
9. Hisanah, N., Subiyanto, S., & Nugraha, A. (2015). Kajian Teknis Penerapan Generalisasi Peta Rupabumi Indonesia (Rbi) Dari Skala 1: 50.000 Menjadi Skala 1:250.000. *Jurnal Geodesi Undip*, *4*(4), 248–256.
10. Kardhana, Y. L. A. W. H. (2013). Aplikasi Sobek Untuk Simulasi Kegagalan Tanggul Laut: Studi Kasus Pluit-Jakarta. *Jurnal Teknik Hidraulik, Vol 4, No 2 (2013): JURNAL TEKNIK HIDRAULIK*, 143–158. http://jurnalth.pusair-pu.go.id/index.php/JTH/article/view/516/380
11. Lukiawan, R., Purwanto, E. H., & Ayundyahrini, M. (2019). Analisis Pentingnya Standar Koreksi Geometrik Citra Satelit Resolusi Menengah Dan Kebutuhan Manfaat Bagi Pengguna. *Jurnal Standardisasi*, *21*(1), 45. https://doi.org/10.31153/js.v21i1.735
12. Mahfudz, M., Riadi, B., & Rifaldi, I. (2022). Pemetaan Area Potensi Banjir Berdasarkan Topographic Wetness Index (TWI) di Kecamatan Cigudeg Kabupaten Bogor. *Jurnal Ilmiah Geomatika*, *28*(1), 13–19.
13. Mangidi, U., Mandaya, I., & Ngii, E. (2023). Utilization of Sentinel 1 SAR for Flood Mapping in North Konawe Regency, Southeast Sulawesi Province, Indonesia. *IOP Conference Series: Earth and Environmental Science*, *1134*(1), 012019. https://doi.org/10.1088/1755-1315/1134/1/012019
14. Nucifera, F., & Putro, S. T. (2018). Deteksi Kerawanan Banjir Genangan Menggunakan Topographic Wetness Index (TWI). *Media Komunikasi Geografi*, *18*(2), 107. https://doi.org/10.23887/mkg.v18i2.12088
15. Park, J. W., Korosov, A. A., Babiker, M., Sandven, S., & Won, J. S. (2018). Efficient Thermal Noise Removal for Sentinel-1 TOPSAR Cross-Polarization Channel. *IEEE Transactions on Geoscience and Remote Sensing*, *56*(3), 1555–1565. https://doi.org/10.1109/TGRS.2017.2765248
16. Rahayu, & Candra, D. S. (2014). Koreksi radiometrik citra landsat-8 kanal Multispektral menggunakan Top of Atmosphere (ToA) untuk mendukung klasifikasi penutup lahan. *In Seminar Nasional Penginderaan Jauh*, *Ldcm*, 762–767.
17. Rubel, O., Lukin, V., Rubel, A., & Egiazarian, K. (2021). Selection of lee filter window size based on despeckling efficiency prediction for sentinel sar images. *Remote Sensing*, *13*(10). https://doi.org/10.3390/rs13101887
18. Tambunan, M. P. (2017). The pattern of spatial flood disaster region in DKI Jakarta. *IOP Conference Series: Earth and Environmental Science*, *56*(1). https://doi.org/10.1088/1755-1315/56/1/012014
19. Taufik, S. R., Yatrib, M., Harman, A. N., Kesuma, T. N. A., Saputra, D., & Kusuma, M. S. B. (2022). Assasment of flood hazard reduction in DKI Jakarta: Bendungan Hilir Village. *IOP Conference Series: Earth and Environmental Science*, *989*(1), 012018. https://doi.org/10.1088/1755-1315/989/1/012018
20. Ulloa, N. I., Chiang, S. H., & Yun, S. H. (2020). Flood proxy mapping with normalized difference Sigma-Naught Index and Shannon's entropy. *Remote Sensing*, *12*(9). https://doi.org/10.3390/RS12091384
21. Wigati, R., & Soedarsono, S. (2016). Normalisasi Sungai Ciliwung Menggunakan Program HEC-RAS 4.1 (Studi Kasus Cililitan - Bidara Cina). *Fondasi : Jurnal Teknik Sipil*, *5*(1), 1–12. https://doi.org/10.36055/jft.v5i1.1242

22. Wijayanti, P., Zhu, X., Hellegers, P., Budiyono, Y., & van Ierland, E. C. (2017). Estimation of river flood damages in Jakarta, Indonesia. *Natural Hazards*, *86*(3), 1059–1079. https://doi.org/10.1007/s11069-016-2730-1

23. Yulihastin, E. (2011). Anomali Curah Hujan 2010 di Benua Maritim Indonesia Berdasarkan Satelit TRMM Terkait. *Prosiding Simposium Nasional Inovasi Pembelajaran Dan Sains*, *June*, 0–5.